Supplementary information

Reverse Hierarchical DED Assembly in the cFLIP-Procaspase-8 and cFLIP-Procaspase-8-FADD Complexes

Chao-Yu Yang[1], Yi-Chun Tseng[1,2,5], Yi-Fan Tu[2,5], Bai-Jiun Kuo[2], Li-Chung Hsu[3,4], Chia-I Lien[3], You-Sheng Lin[3], Yin-Ting Wang[1], Yen-Chen Lu[2], Tsung-Wei Su[1], Yu-Chih Lo[2,*], Su-Chang Lin[1,*]

[1]Genomics Research Center, Academia Sinica, Taipei 11529, Taiwan

[2]Department of Biotechnology and Bioindustry Sciences, College of Bioscience and Biotechnology, National Cheng Kung University, Tainan 70101, Taiwan

[3]Institute of Molecular Medicine, College of Medicine, National Taiwan University, Taipei 10002, Taiwan

[4]Center of Precision Medicine, College of Medicine, National Taiwan University, Taipei 10002, Taiwan

[5]These authors contributed equally

---

*Correspondence to:

Yu-Chih Lo, gracelo@ncku.edu.tw

Su-Chang Lin, tomlin@gate.sinica.edu.tw

Supplementary Figures

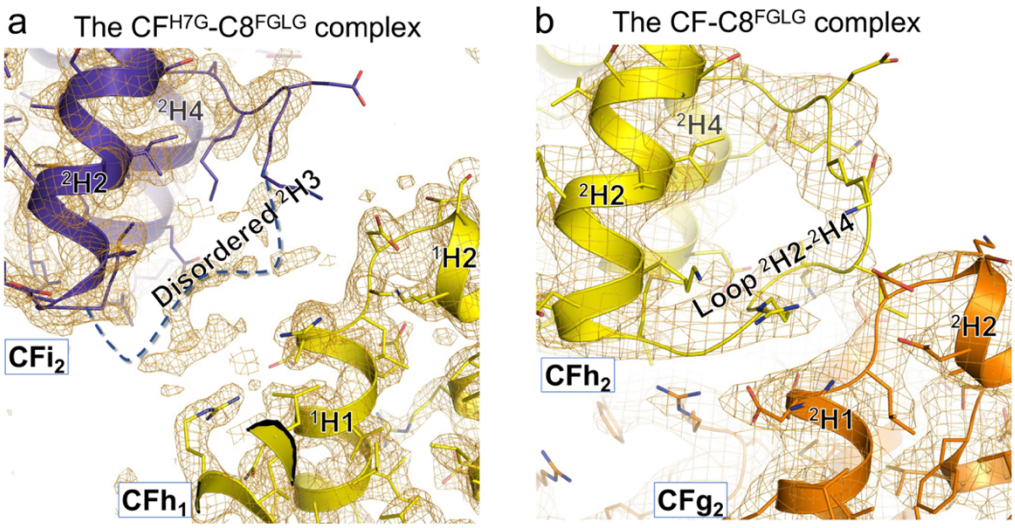

c Sequence identity (= the identical residues/aligned residues), based on the structure-based sequence alignment in Supplementary Fig. 1a of Yang et al. (10.1038/s41467-024-47990-2).

	Casp-8 DED1	Casp-8 DED2	cFLIP DED1	cFLIP DED2
FADD DED	28/82=34.1%	21/82=25.6%	23/75=30.6%	21/83=25.3%
Casp-8 DED1		21/81=25.9%	23/84=27.3%	24/84=28.5%
Casp-8 DED2			14/86=16.2%	22/74=29.7%
cFLIP DED1				17/76=22.3%

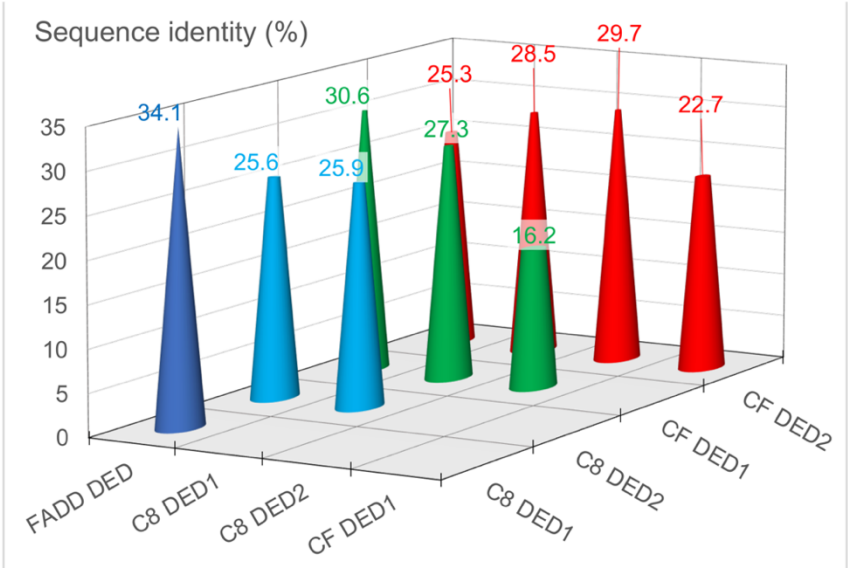

Supplementary Fig. 1 Representative electron density maps for the binary CF-C8^{FGLG} and CF^{H7G}-C8^{FGLG} complexes. a The 2Fo-Fc electron density map for the CF^{H7G}-C8^{FGLG} complex, contoured at 1.5 sigma using PyMol, shows a region containing the type III interface

between DED2 of cFLIP molecule CFi and DED1 of cFLIP molecule CFh as seen in Fig. 3g. The ribbons illustrate the atomic coordinates. This region contains a disordered helix, ^{2}H3, represented by a dotted line, in cFLIP DED CFi_2. The disordered helix ^{2}H3 is referred to as a disordered loop ^{2}H2-^{2}H4 in (**b**). Helices 1 to 7 of each DED are numbered H1 to H7, while ^{2}H4 stands for the helix 4 in DED2. See the figure legend of Fig. 1c for the naming convention. **b** Similar to (a), but shows the 2Fo-Fc electron density map for the CF-$C8^{FGLG}$ complex. This map illustrates a region containing the type III interface between DED2 of cFLIP molecules CFh and CFg as seen in Fig. 3g. Notably, this region contains a more ordered loop ^{2}H2-^{2}H4 of cFLIP DED CFh_2, compared to the disordered loop ^{2}H2-^{2}H4 of cFLIP DED CFi_2 in (**a**). **c** The sequence identity among FADD DED, Casp-8 DED1, Casp-8 DED2, cFLIP DED1, and cFLIP DED2. The identity was estimated based on the structure-based sequence alignment in Supplementary Fig. 1a of Yang et al. (10.1038/s41467-024-47990-2)[1]. (n=1 data) Source data are provided as a Source Data file.

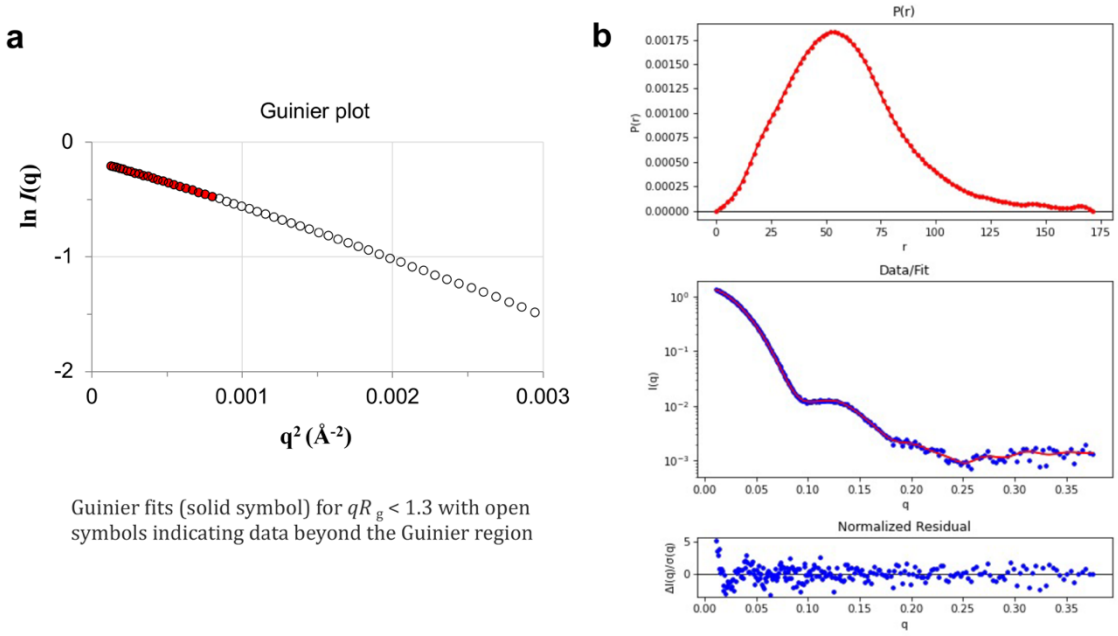

Supplementary Fig. 2: The SAXS data for the CF-C8^{FGLG} complex. a The Guinier plot for the SAXS data shown in Fig. 2d. **b** *P*(*r*) analysis and fit of SAXS data to the model in Fig. 2d. See also Supplementary Table 2.

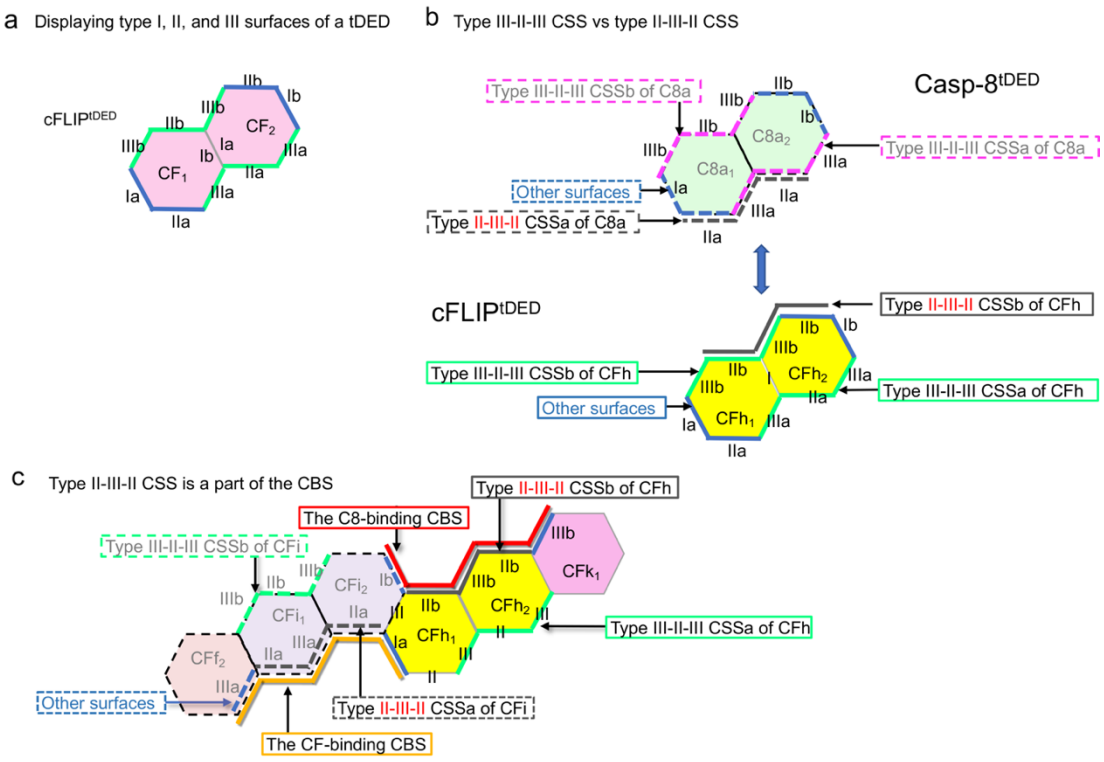

Supplementary Fig. 3 Different types of the surfaces and CSS on tDED. a Displays the type Ia, Ib, IIa, IIb, IIIa, and IIIb surfaces of tDED using cFLIP tDED as an example. **b** Displays different type of the CSS surfaces of cFLIP and Casp-8 tDED. Pink, green, or dark grey angled and angled/dashed lines represent different CSS of tDEDs. **c** Illustrates that type II-III-II CSS is a part of the CBS for the protein-protein interaction between the molecules of different layers. For comparison, type III-II-III CSS is mainly involved in self-assembly occurring in the same layer. The molecules are colored as their counterparts in Fig. 3g. $C8d_1$ denotes DED1 of Casp-8^{tDED} chain d, while CFf represents cFLIP^{tDED} chain f.

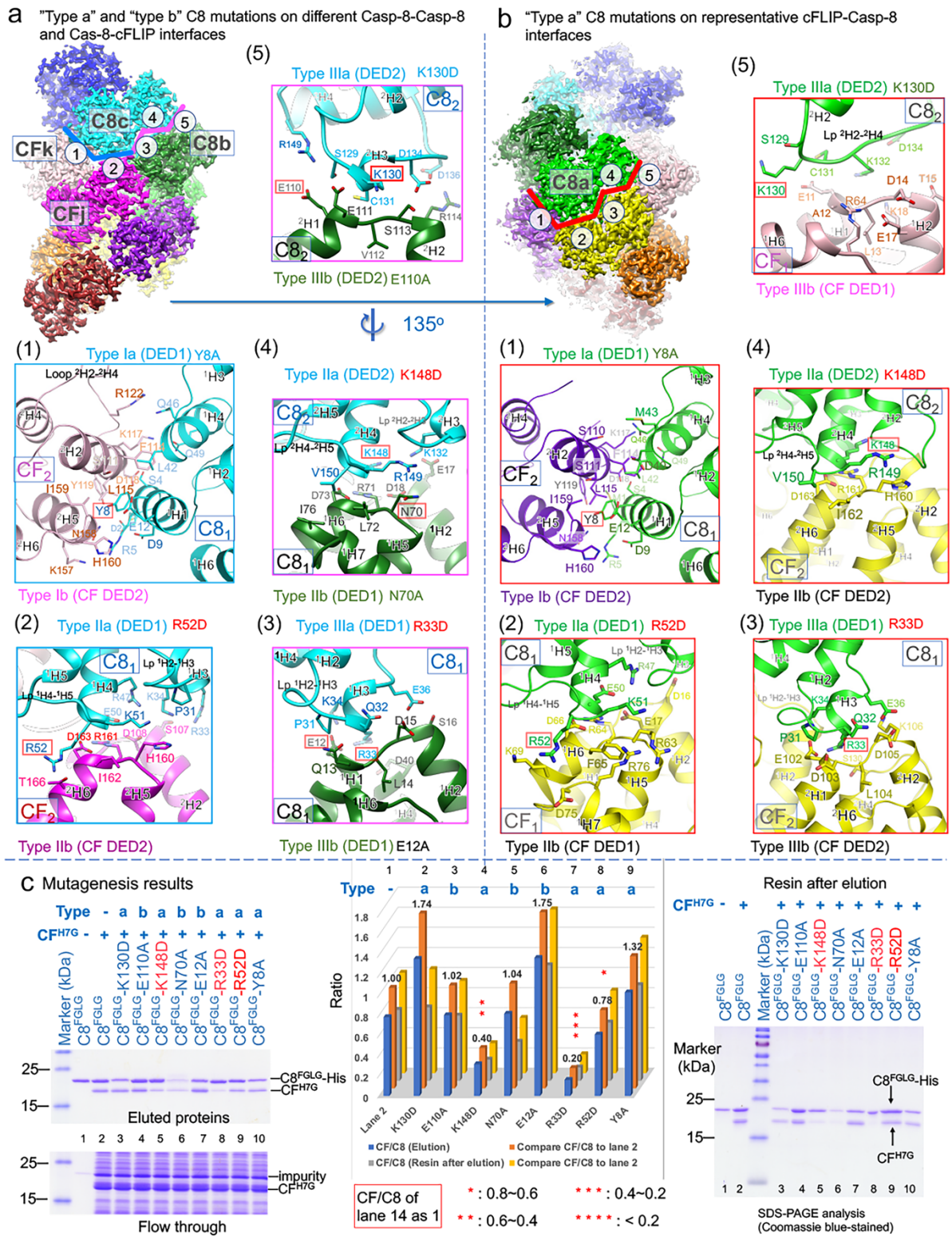

Supplementary Fig. 4 Casp-8^{tDED} self-assembly plays a minor role in the formation of the CF^{H7G}-C8^{FGLG} complex. a Displays five representative interfaces involved in the Casp-8-Casp-8 and cFLIP-Casp-8 interactions within the CF^{H7G}-C8^{FGLG} complex. The interface

residues and the Casp-8 mutations generated in this study are indicated for each interface. Thick pink lines illustrate the type III-II-III interface between two Casp-8^{tDED} molecules, while thick blue lines represent the representative interfaces between a type III-II-III CSS-mediated cFLIP^{tDED} trimer and a Casp-8^{tDED} molecule. The molecules are colored as their counterparts in Fig. 3g. $C8_1$ denotes DED1 of Casp-8^{tDED}, while CFf represents cFLIP^{tDED} chain f**. b** Depicts the five interfaces involved in the interaction between the cFLIP double-layer intermediate complex and Casp-8 within the same complex. Red thick lines indicate the Casp-8-recruiting CBS on the cFLIP double-layer intermediate complex. The interface residues and the Casp-8 mutations generated in this study are illustrated for each interface. **c** Pulldown of CF^{H7G} by His-tagged C8^{FGLG} or mutant C8^{FGLG} to evaluate the importance of the C8 self-assembly in the binary complex formation. The resin-bound fractions are divided into the eluted protein fractions (shown here) and the resin after elution fractions (shown in (**d**)). Both fractions underwent SDS-PAGE analysis to access the amount of bound CF and His-tagged C8^{FGLG}, with each band quantified using ImageJ (https://imagej.net/ij/)[2]. The bar chart shows the quantified mutagenesis results of (**c**) and (**d**) (therefore, n=1 data), with the ratios of cFLIP to Casp-8 plotted as blue and light blue bars for the eluted protein and resin after elution fractions, respectively. Each ratio is normalized to that of lane 14, with the normalized results plotted as orange and yellow bars, respectively, and the ratio shown on top. "Type a" and "type b" Casp-8 mutations are indicated. The flow-through fractions are also shown here.**d** Shows the SDS-PAGE analysis results of the resin after elution fractions from (**c**). Source data are provided as a Source Data file. The experiments were repeated twice with similar results.

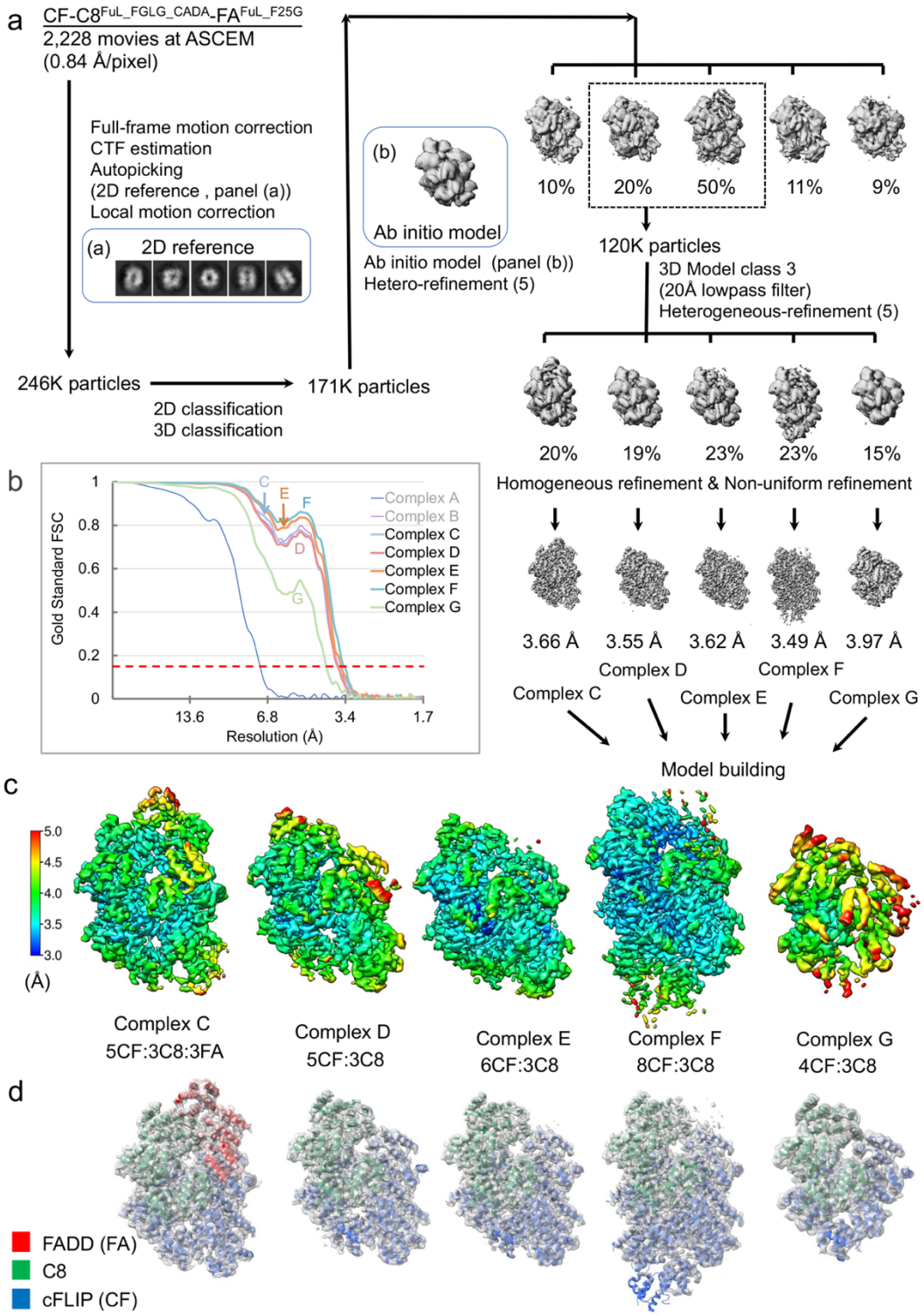

Supplementary Fig. 5 The procedure of cryo-EM structure determination. a Diagrams illustrating the structure determination process for the CF-C8^{FuL_FGLG_CADA}-FA^{FuL_F25G} complex, resulting in five cryo-EM models: one ternary complex (Complex C) and four binary complexes (Complexes D to G). See also Supplementary Figs. 6, 7. **b** The corresponding

Fourier Shell Correlation (FSC) curves for Complexes C to G. FSC curves for the Complexes A (EMD-39127 [https://www.ebi.ac.uk/pdbe/entry/emdb/EMD-39127]) and B (EMD-39126 [https://www.ebi.ac.uk/pdbe/entry/emdb/EMD-39126]) of the CF-C8^{FuL_FGLG_CADA}-FA^{FuL} complex[1] are shown for comparison. **c** Local resolution mapped onto the cryo-EM envelope of each complex solved in (**a**). **d** Overview of the atomic coordinates of the binary cFLIP-Casp-8 tDED and ternary cFLIP-Casp-8-FADD DED complexes fit into the corresponding cryo-EM density maps. FADD is colored in red, while Casp-8 and cFLIP are colored in green and blue, respectively.

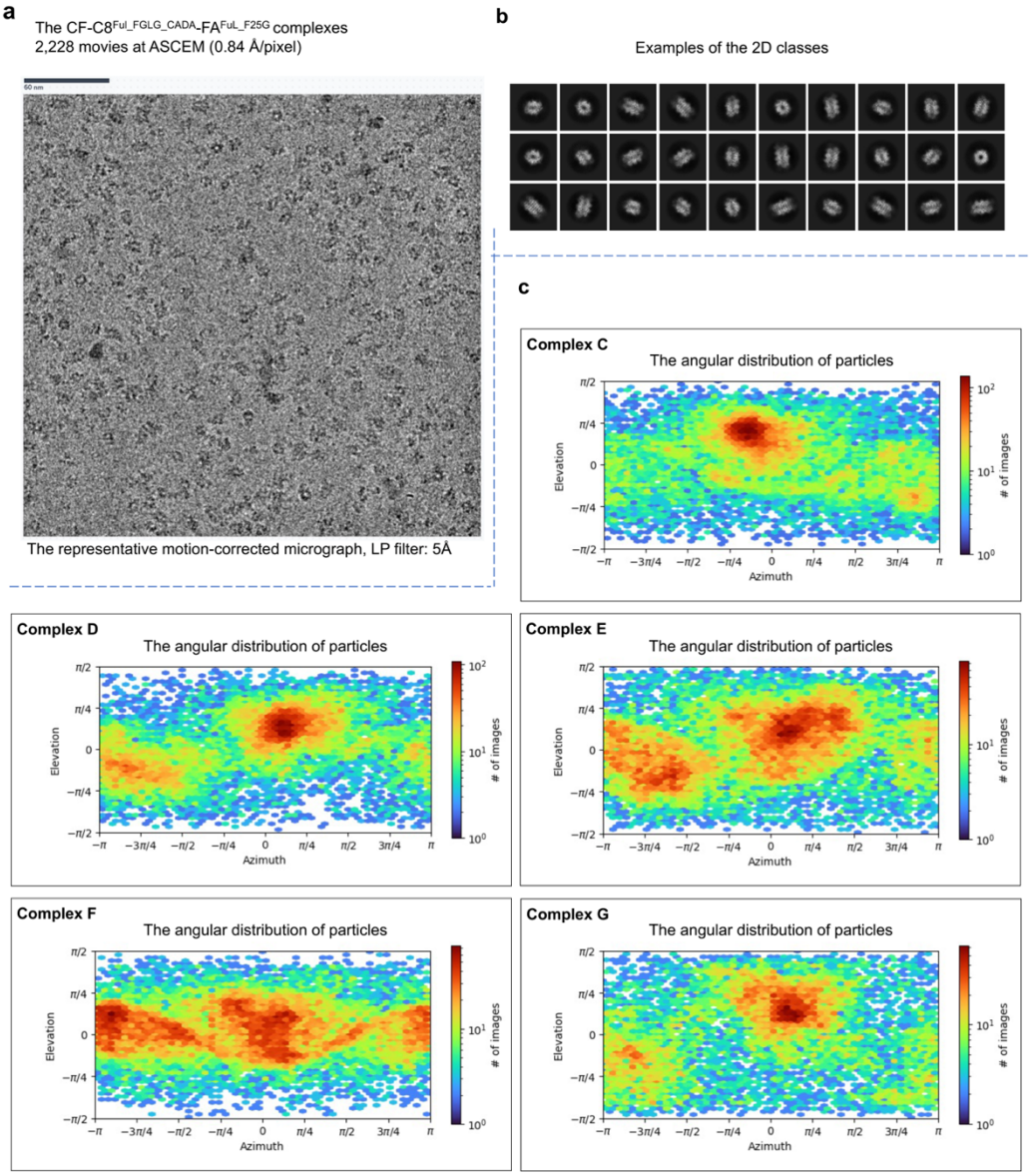

Supplementary Fig. 6 Representative cryo-EM micrographs, 2D classes, and angular distribution of particles from the ternary CF-C8^{FuL_FGLG_CADA}-FA^{FuL_F25G} complex. a Representative Cryo-EM micrograph for the CF-C8^{FuL_FGLG_CADA}-FA^{FuL_F25G} complex. Scale bar = 60 nm. Thousands of movies were collected to produce micrographs with similar results. Source data are provided as a Source Data file. **b** Examples of 2D classes for the particles from the CF-C8^{FuL_FGLG_CADA}-FA^{FuL_F25G} complex. **c** Angular distribution of particles in the cryo-EM analysis of the Complexes C to G. See also Supplementary Fig. 5.

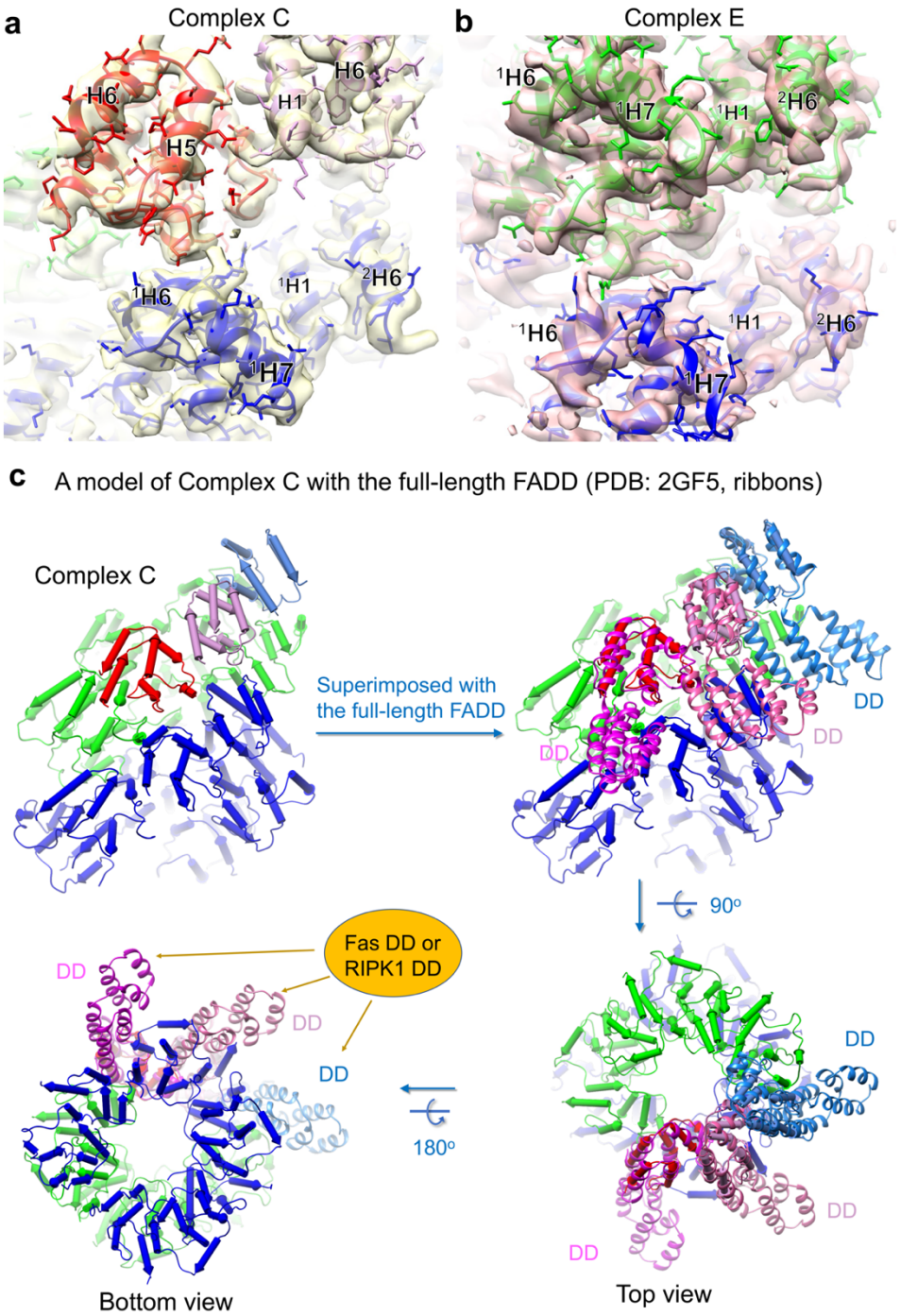

Supplementary Fig. 7 Representative cryo-EM envelopes reconstituted from the ternary CF-C8^{FuL_FGLG_CADA}-FA^{FuL_F25G} complex. a The cryo-EM envelop of the Complex C shows the region where the 1st and 2nd FADD molecules are recruited by the binary cFLIP-Casp-8 complex. The envelopes clearly identify FADD due to the absence of density for helix H7, while helix ^{1}H7 of cFLIP tDED (blue ribbons) is present. The 1st and 2nd FADD molecules, FAl and FAr, are colored in red and pink, respectively. Casp-8 and cFLIP are colored in green

and blue, respectively. **b** The cryo-EM envelop of the complex E shows the region where the first Casp-8 molecule (C8a) is recruited by the cFLIP oligomeric complex. Casp-8 and cFLIP are colored in green and blue, respectively. The lower part includes the envelops for helix ^{1}H7 of cFLIP (blue ribbons). Please note that the upper part contains the envelops for a helix ^{1}H7 (green ribbons), helping confirming the identity of Casp-8 tDED, especially in comparison to the FAl and FAr region shown in (**a**). **c** A model of Complex C (in pipes-and-planks) with the full-length FADD (in ribbons). The DED of the full-length FADD (PDB: 2GF5 [http://doi.org/10.2210/pdb2GF5/pdb], Carrington et al. 10.1016/j.molcel.2006.04.018)[3] was superimposed with the FADD DED of Complex C in order to predict the locations of FADD DD for interacting with Fas DD or RIPK1 DD (orange arrows). For the possible location of Casp-8's caspase domain and its heterodimer with cFLIP's pseudo-caspase domain, please refer to Figs. 5c, 7b, and 7c in Yang et al. 10.1038/s41467-024-47990-2.[1] The molecules are colored as their counterparts in Fig. 7.

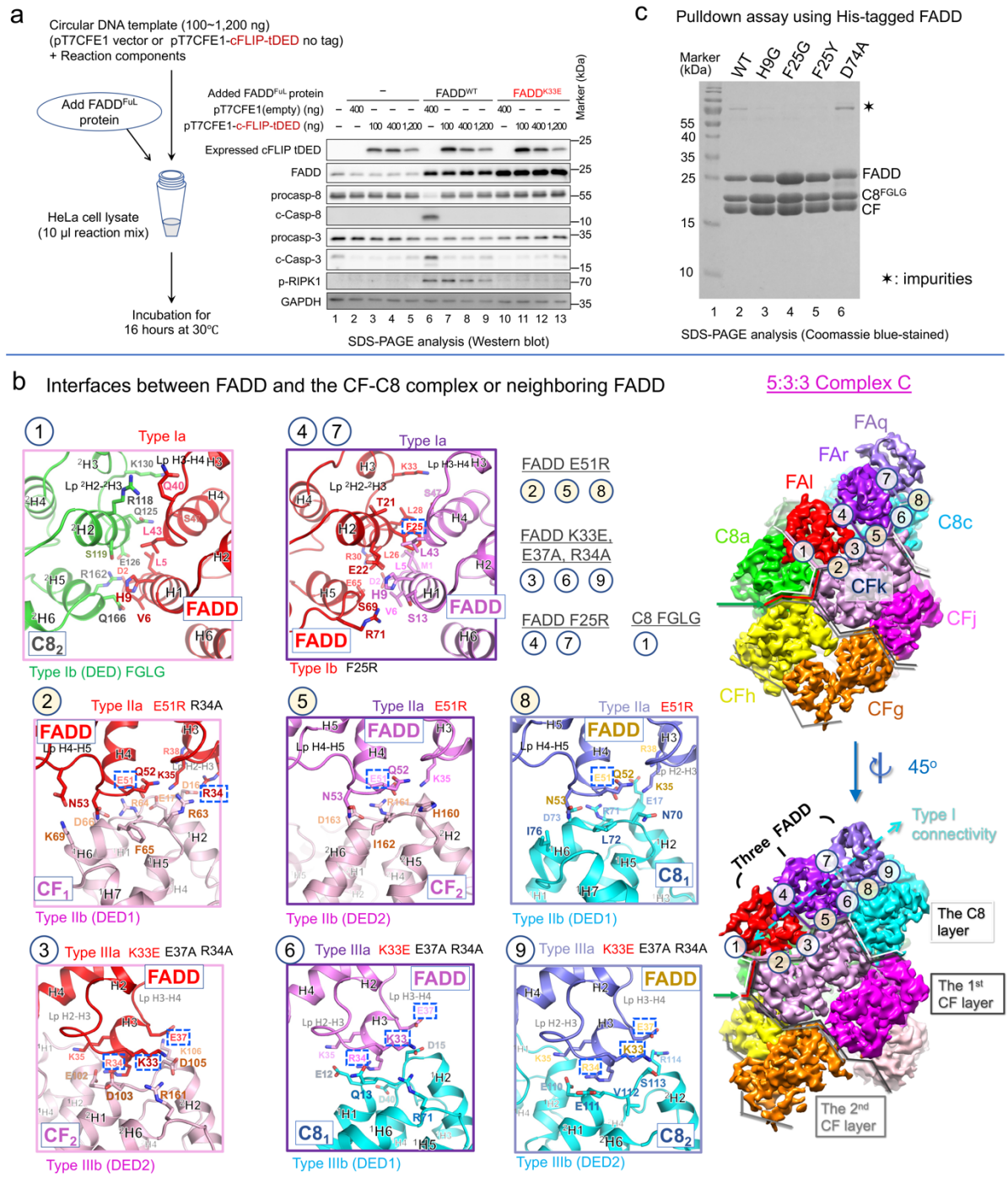

Supplementary Fig. 8 The effects of FADD mutations on the reverse hierarchical binding process. a Cell-lysate based mutagenesis results. FADD protein and varying amounts of cFLIP^{tDED}-expressing plasmid were simultaneously added to HeLa cell lysate for a 16-hour incubation. The effects of the FADD K33E mutation and the absence of cFLIP's pseudo-caspase domain were examined by western blotting. Lane 6 shows that the addition of FADD simultaneously induces two functionally different complexes: Casp-8 activation and RIPK1

activation. Expressed cFLIP^{tDED} inhibits added-FADD-induced Casp-8 but not RIPK1 activation (Lane 7). The western blotting data were repeated twice with similar results. **b** Residues involved in the seven interfaces between FADD and the binary CF-C8 complex, and the two interfaces between FADD and neighboring FADD in the triple-FADD complex, as mentioned in Fig. 6e. Nine boxes represent the nine representative interfaces, with their locations highlighted on the molecular surfaces of the 5:3:3 Complex C. The locations of various FADD mutations and Casp-8 FGLG mutations on different interfaces are highlighted. In each box, interface residues are shown in stick presentation, with FADD mutations highlighted by dashed boxes. FADD mutations that inhibit expressed-cFLIP-induced Casp-8 activation are labeled in red. The molecular surfaces are the cryo-EM envelops for the Complex C. Green arrows point to the CBS, illustrated by red lines, originally on the cFLIP double-layer intermediate complex for recruiting Casp-8 molecule C8a. White and grey lines show the Casp-8 layer or cFLIP layers. $C8_1$ denotes DED1 of Casp-8^{tDED}, while CFf represents cFLIP^{tDED} chain f. **c** SDS-PAGE analysis results for reconstituting ternary cFLIP^{tDED}-Casp-8^{tDED_FGLG}-FADD^{FuL} complexes with different FADD mutants in reverse order, using the method described in Fig. 5a. Ni-resin loaded with various His-tagged FADD mutants was used to pulldown the tag-removed, double-purified binary CF-C8^{FGLG} complex. Subsequently the Ni-resin was washed and subjected to SDS-PAGE analysis. The experiments were repeated twice with similar results. Source data are provided as a Source Data file.

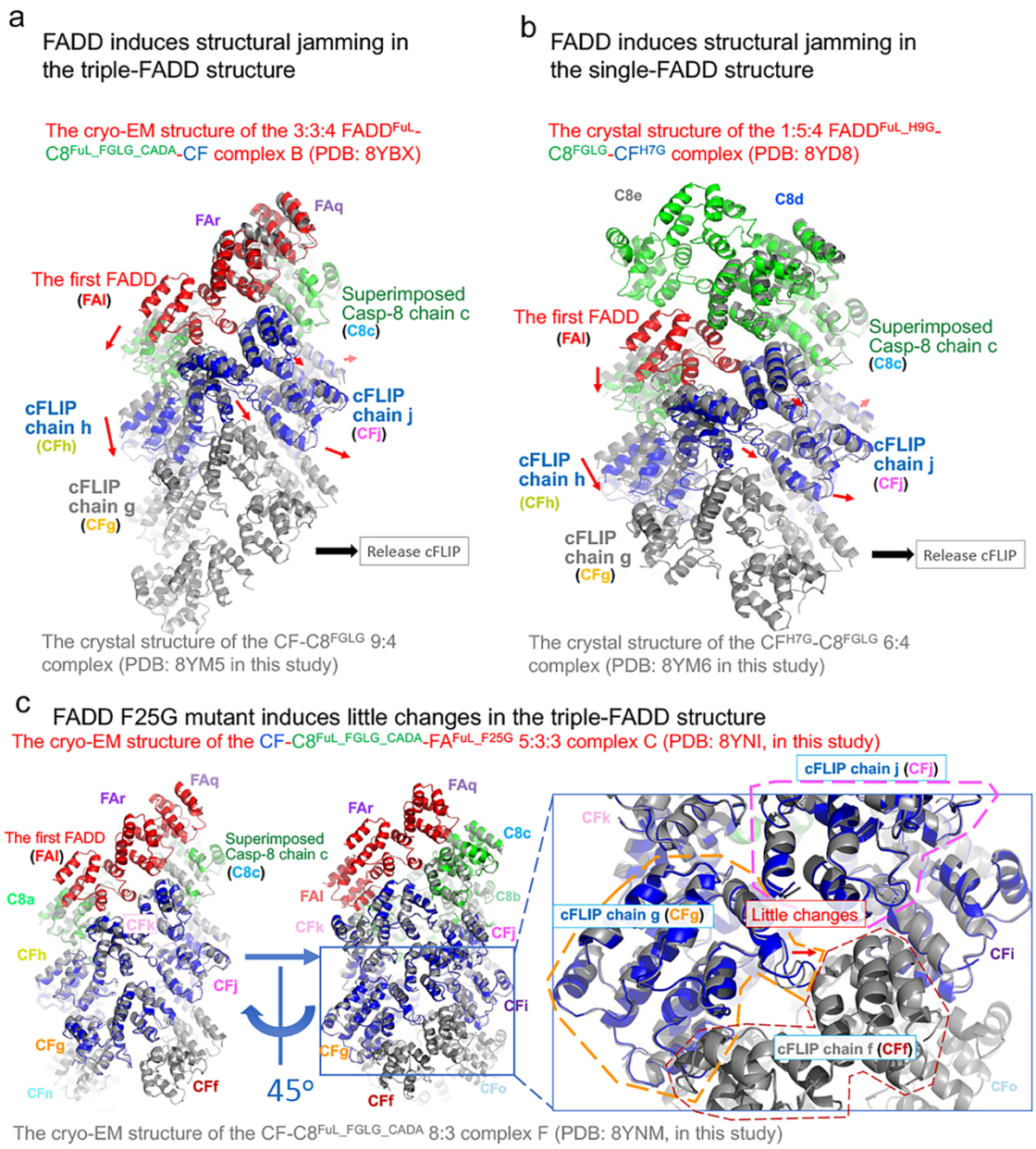

Supplementary Fig. 9 The presence of FADD alters the cFLIP-Casp-8 tDED assembly. a-c Structural comparison of the binary complex (grey) and corresponding ternary complex (colored as their counterparts in Fig. 5h). Red arrows indicate shifts in tDED relative to the superimposed Casp-8 molecule C8c. **a** The comparison suggests that the presence of triple-FADD in the ternary complex transforms the CF-C8 assembly into a CF-C8 hetero-double layer, different from the binary complex. **b** The comparison indicates that the presence of single-FADD also causes structural jamming, resulting in a CF-C8 hetero-double layer in the

ternary complex. **c** The comparison shows that the recruitment of the FADD F25G mutant induces minimal changes in CF-C8 tDED assembly, as highlighted in the close-up view. The transition from a CF triple-layer to a CF-C8 hetero-double layer is incomplete, with cFLIP molecule CFg remaining in the complex. CFf represents cFLIP^{tDED} chain f.

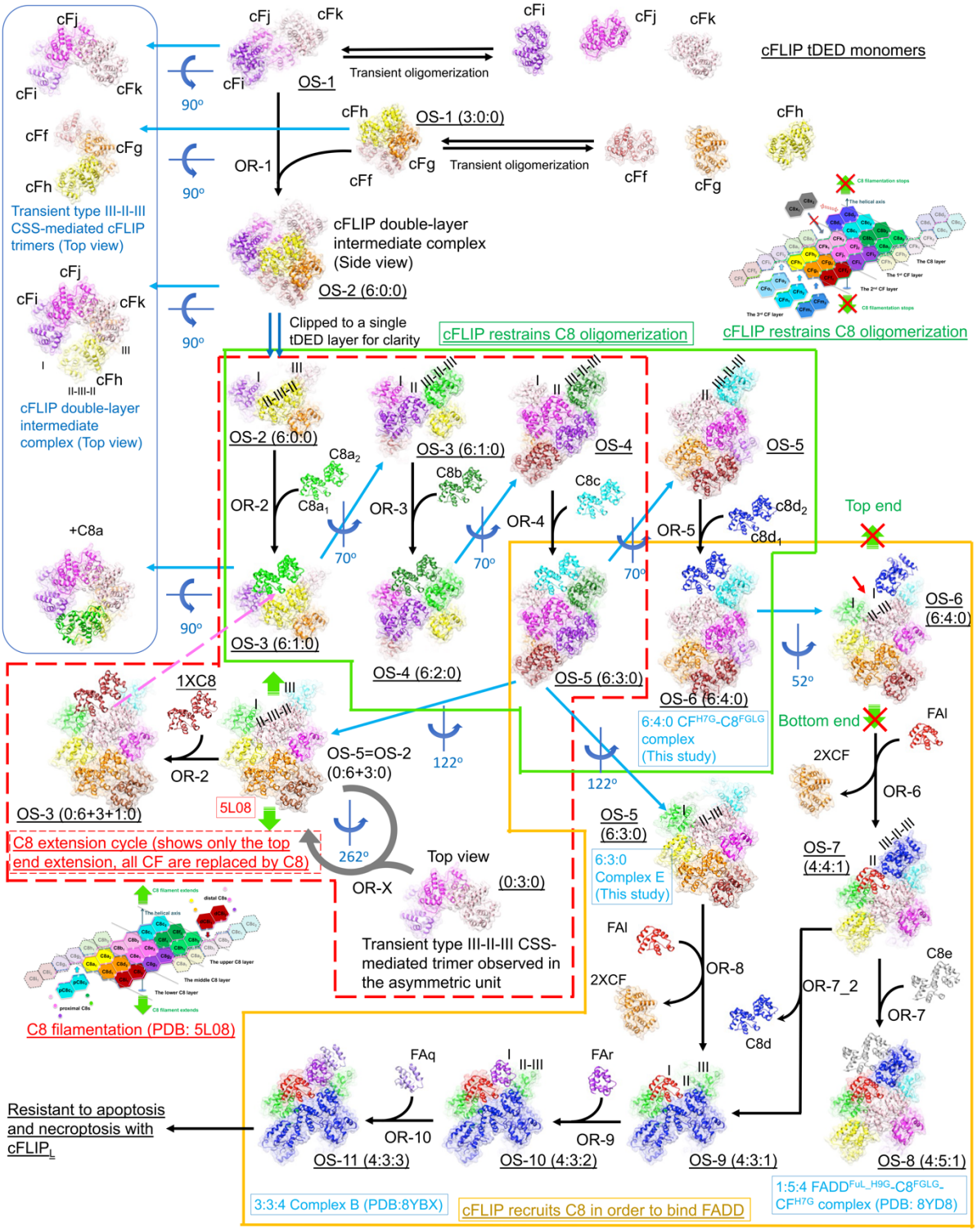

Supplementary Fig. 10 Proposed mechanisms for the assembly of DED complexes between cFLIP, Casp-8, and FADD in reverse order. Black arrows represent oligomerization reactions (OR) that result in an intermediate or stable complexes at specific oligomerization states (OS). Blue arrows indicate rotations by a certain degree. The molecules

are colored as their counterparts in Figs. 1d, 3g, and 5h. $C8d_1$ denotes DED1 of Casp-8^{tDED} chain d, while CFf represents $cFLIP^{tDED}$ chain f.

Elevated levels of cFLIP could form a transient type III-II-III CSS-mediated trimer (OS-1) with a CF:C8:FA ratio of 3:0:0. In OR-1, two transient trimers merge to form a more stable double-layer intermediate complex (OS-2, 6:0:0), creating a CBS with a type I interface, a type II-III-II CSS, and a type III interface. In OR-2, OS-2 recruits a Casp-8 molecule to form OS-3 (6:1:0). Subsequently, in OR-3 and subsequent OR-4, OS-3 (6:1:0) and OS-4 (6:2:0) recruit additional Casp-8 molecules, resulting in OS-4 (6:2:0) and OS-5 (6:3:0), respectively. To restrain C8 oligomerization (in the green box), OS-5 recruits the 4^{th} Casp-8 molecule (C8d) to form OS-6 (6:4:0) in OR-5.

The resultant CF-C8 complex could bind FADD (in the orange box). In OR-6, OS-6 binds a FADD molecule and loses two cFLIP molecules to form OS-7 (4:4:1). In OR-7 or OR7_2, OS-7 recruits or loses a Casp-8 molecule to form OS-8 (4:5:1) or OS-9 (4:3:1), respectively. Alternatively, OS-5 can sequentially recruit three FADD and lose two cFLIP molecules to form Complex B (OS-11, 4:3:3) through OR-8 to OR-10.

For comparison, the mechanism of C8 filamentation on the top end is shown in the red dashed box. Assuming that Casp-8 form OS-2 (0:6:0), it enters the C8 filamentation cycle to sequentially recruit three Casp-8 molecules, forming OS-5 (0:6+3:0). OS-5 is essentially a longer version of OS-2 with the same CBS. It can recruit a Casp-8 molecule (via OR-2) to form OS-3 to repeat the C8 filamentation cycle (indicated by a dotted pink arrow) or recruit any existing C8 transient trimer repeatedly (OR-X, shown by a grey arrow) in filament extension.

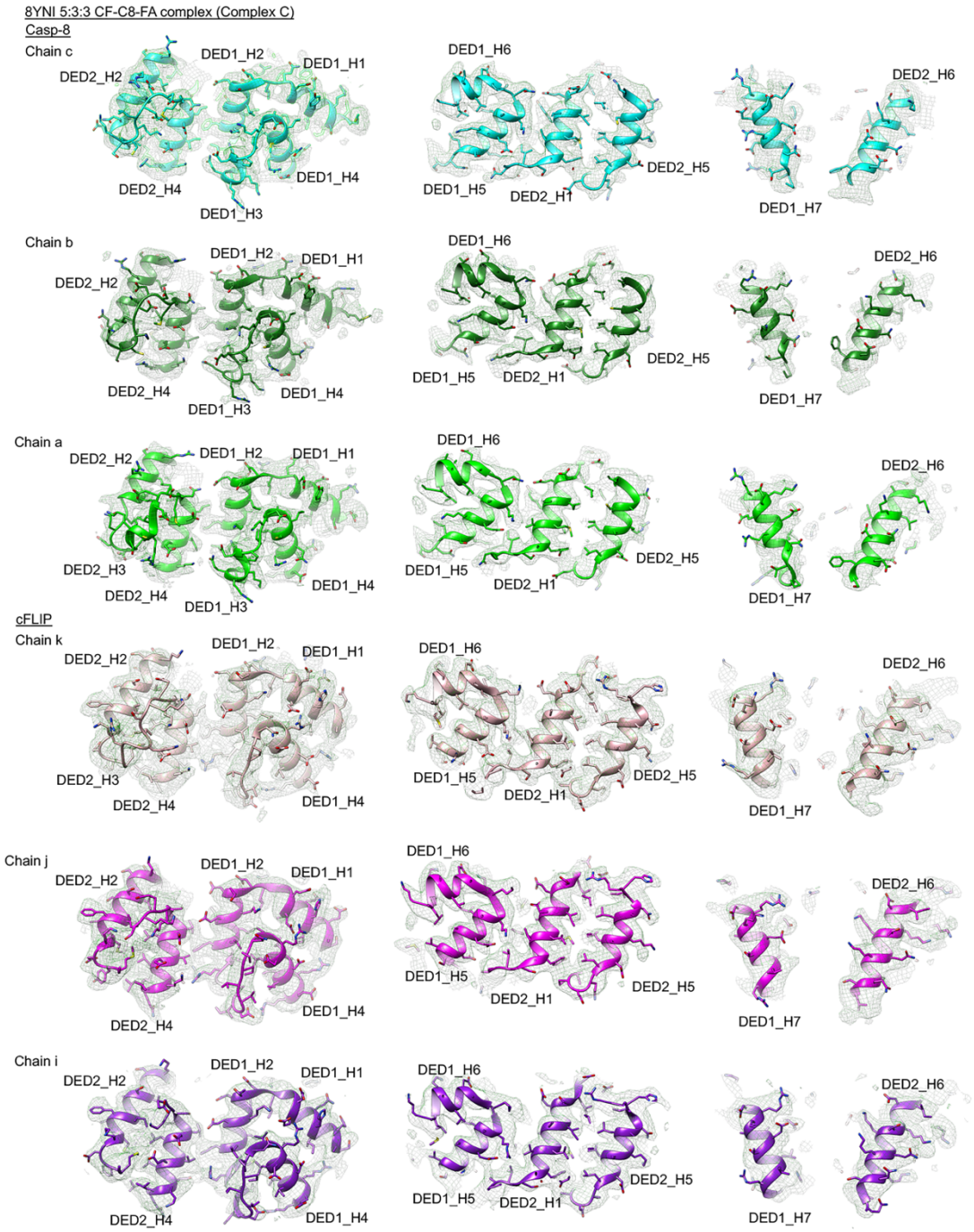

Supplementary Fig. 11: Cryo-EM maps for each helix of DED in Complex C

Figure and figure legend continue on the following page.

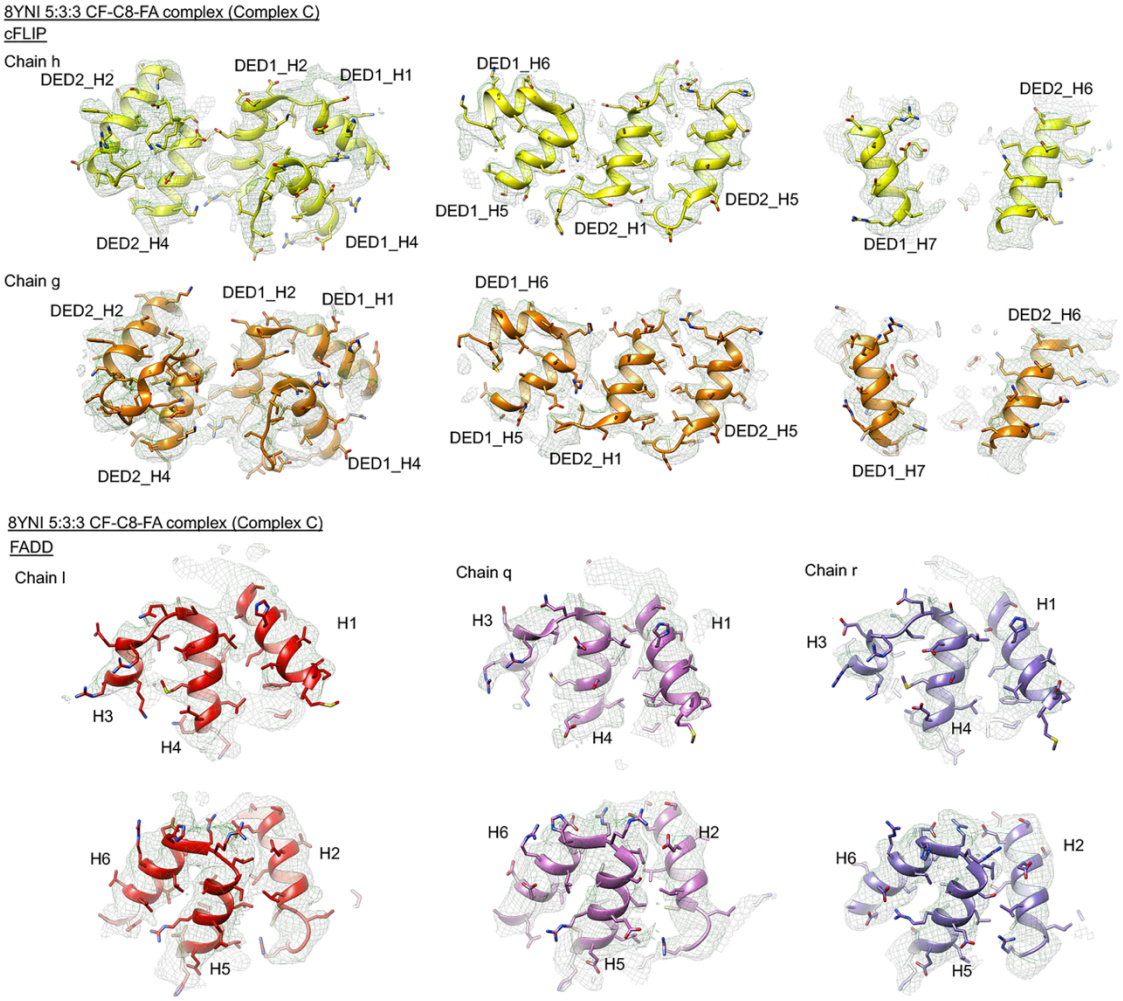

Supplementary Fig. 11: Cryo-EM maps for each helix of DED in Complex C

Shows cryo-EM maps for each helix of DED in the cryo-EM structure of 5:3:3 CF-C8-FA complex (Complex C). The contour level of the surface: 0.20-0.24 (about sdlevel 18-24) using UCSF Chimera version 1.16-42360.

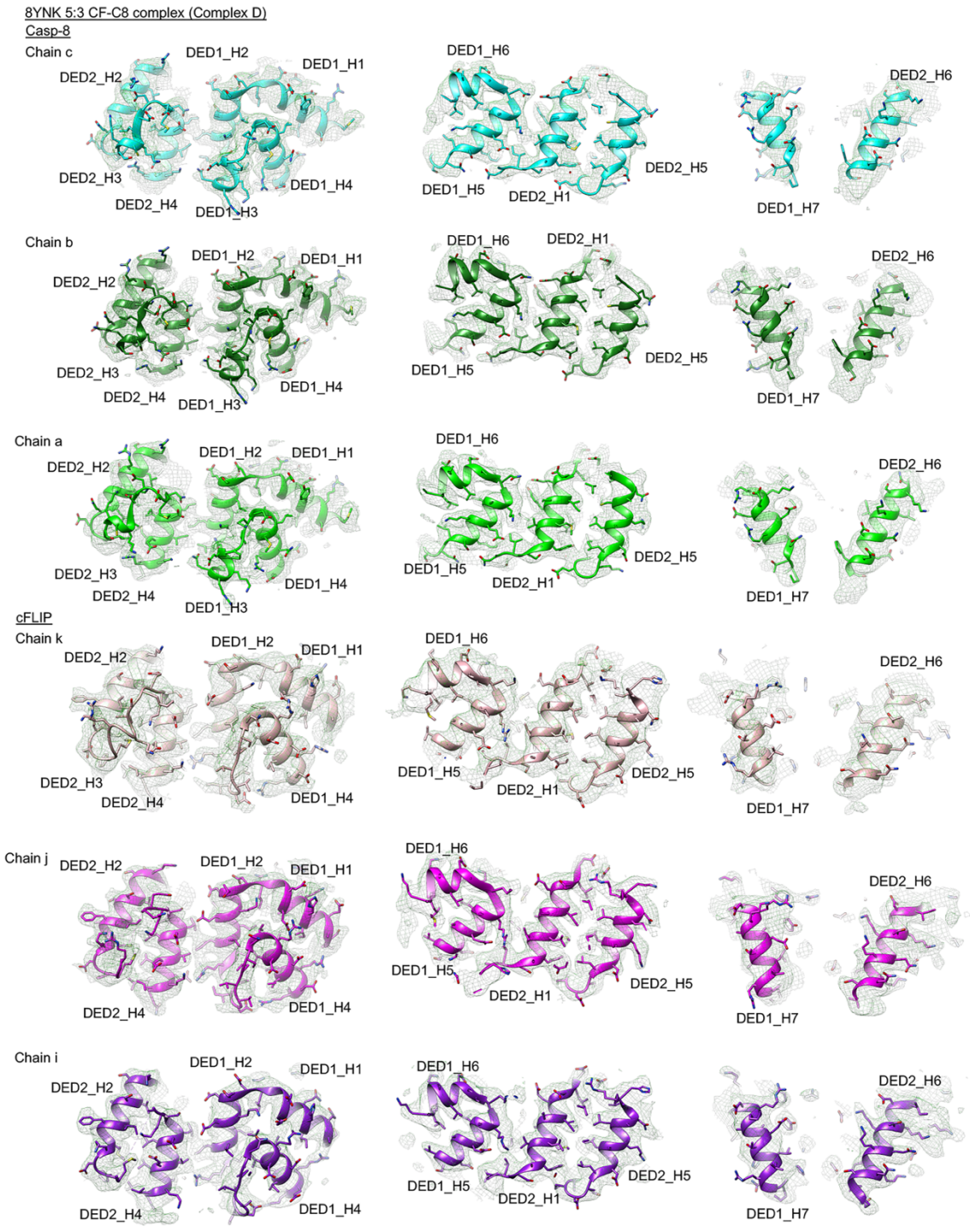

Supplementary Fig. 12: Cryo-EM maps for each helix of DED in Complex D

Figure and figure legend continue on the following page.

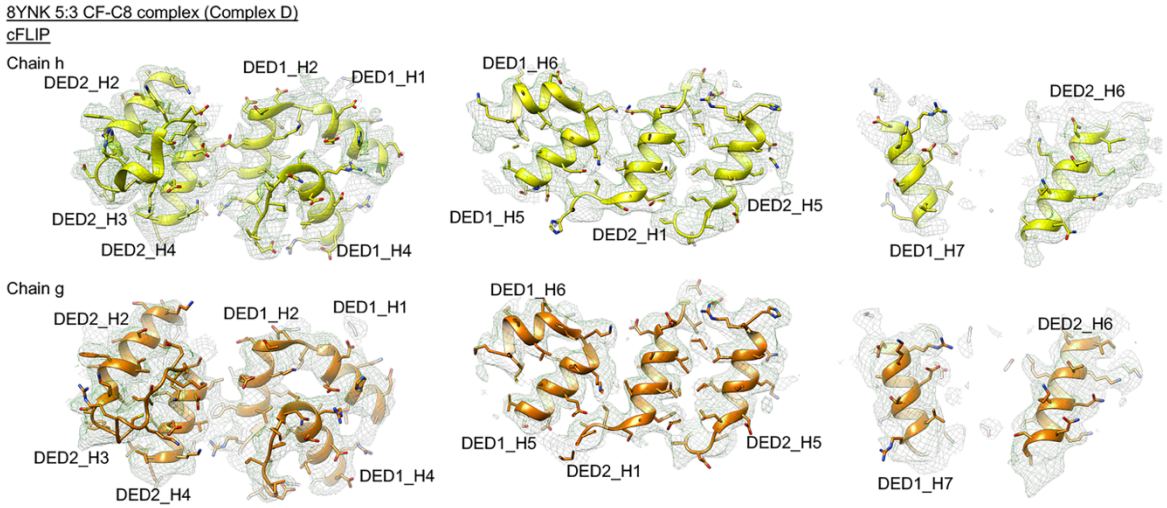

Supplementary Fig. 12: Cryo-EM maps for each helix of DED in Complex D

Shows cryo-EM maps for each helix of DED in the cryo-EM structure of 5:3 CF-C8 complex (Complex D). The contour level of the surface: 0.20-0.24 (about sdlevel 18-24) using UCSF Chimera version 1.16-42360.

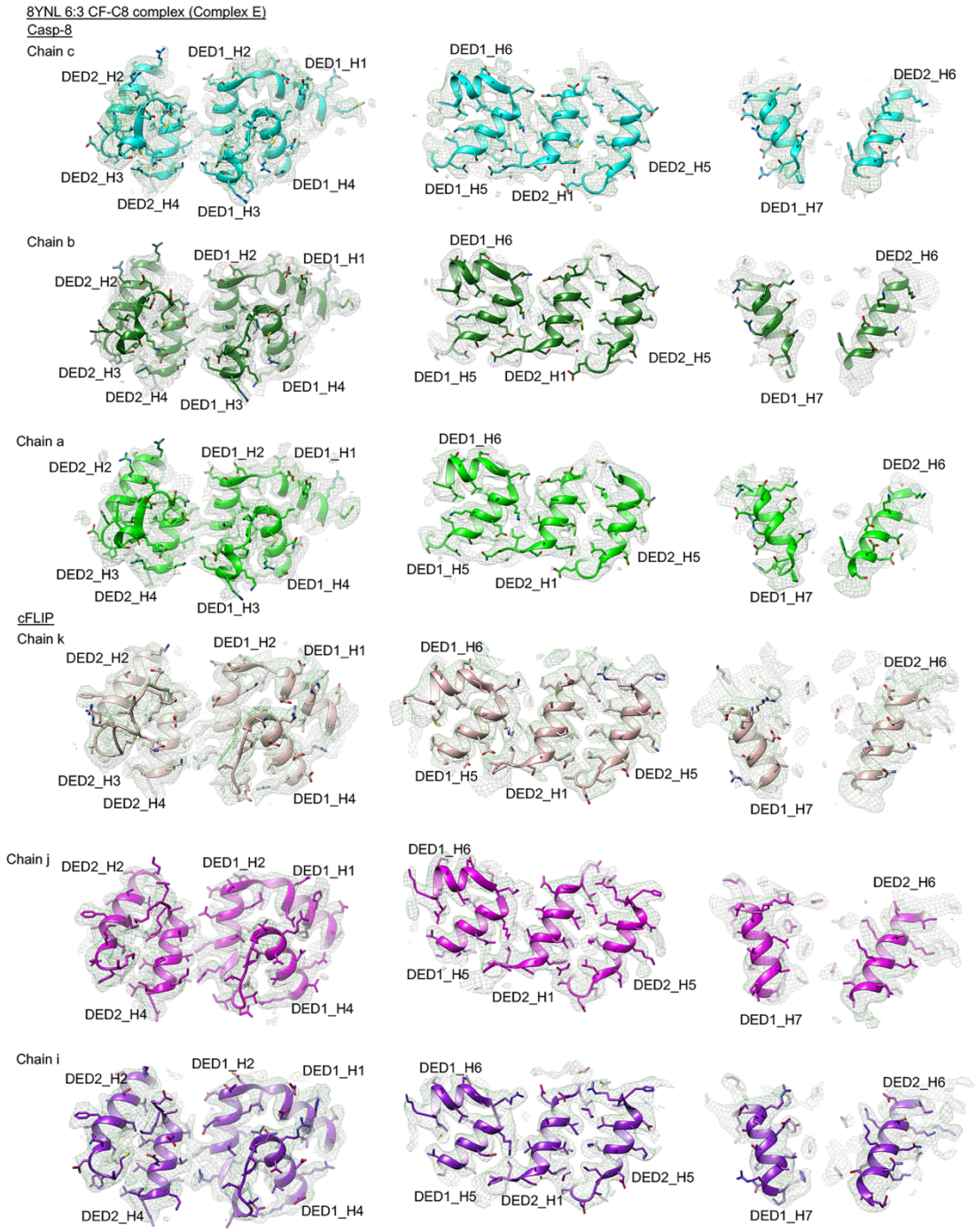

Supplementary Fig. 13: Cryo-EM maps for each helix of DED in Complex E

Figure and figure legend continue on the following page.

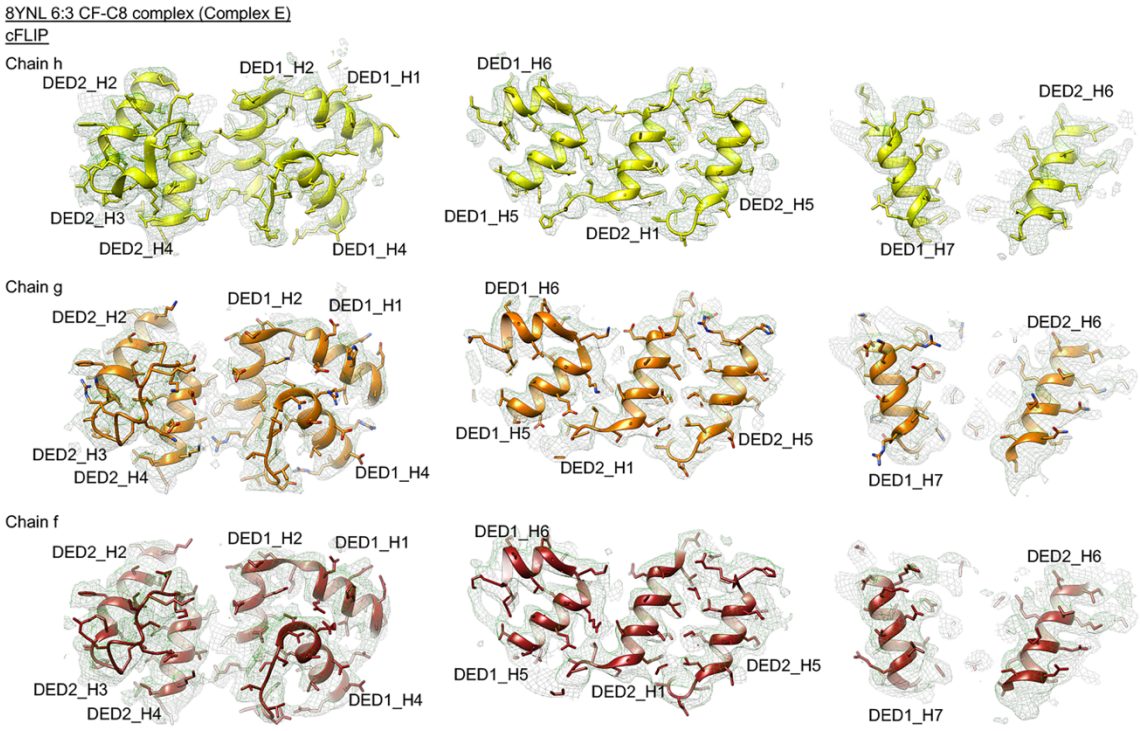

Supplementary Fig. 13: Cryo-EM maps for each helix of DED in Complex E

Shows cryo-EM maps for each helix of DED in the cryo-EM structure of 6:3 CF-C8 complex (Complex E). The contour level of the surface: 0.20-0.24 (about sdlevel 18-24) using UCSF Chimera version 1.16-42360.

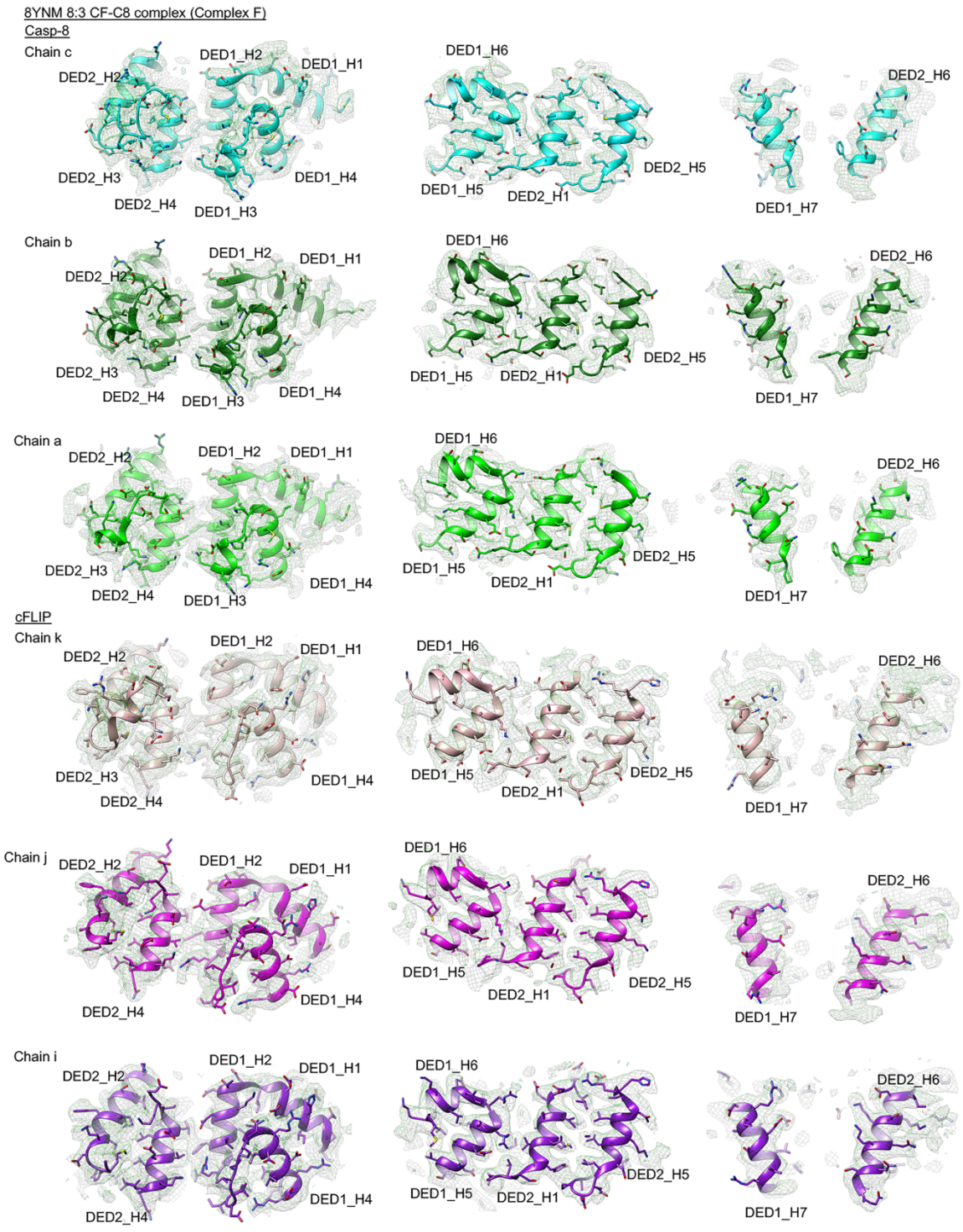

Supplementary Fig. 14: Cryo-EM maps for each helix of DED in Complex F

Figure and figure legend continue on the following page.

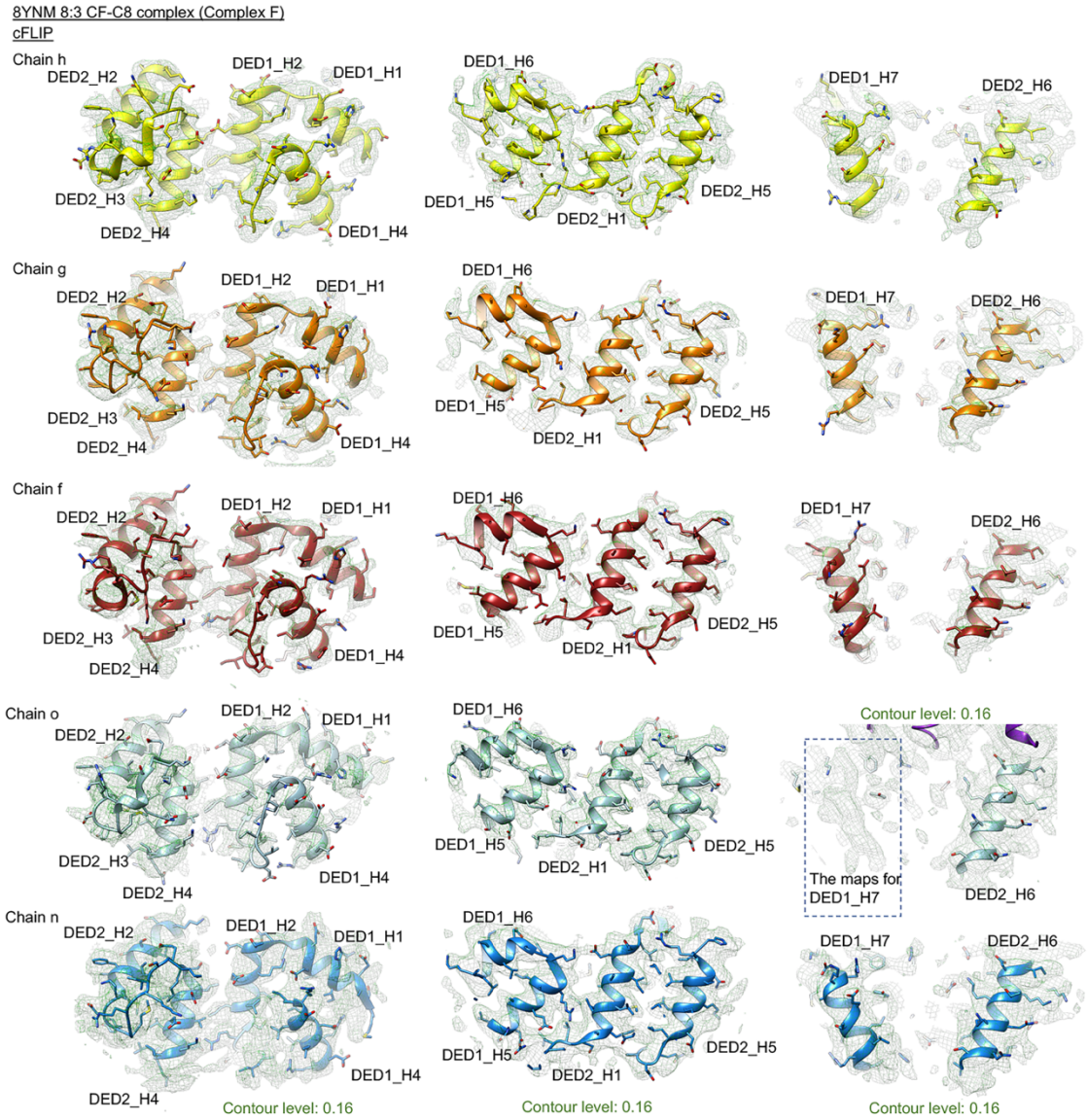

Supplementary Fig. 14: Cryo-EM maps for each helix of DED in Complex F

Shows cryo-EM maps for each helix of DED in the cryo-EM structure of 8:3 CF-C8 complex (Complex F). The contour level of the surface: 0.20-0.24 (unless specified in figure) using UCSF Chimera version 1.16-42360. Notably, the corresponding cFLIP tDED chains o and n in the crystal structure of the CF-C8_FGLG complex (PDB 8YM6 in this study) have electron density maps for building all helices including DED1_H7 of chain o.

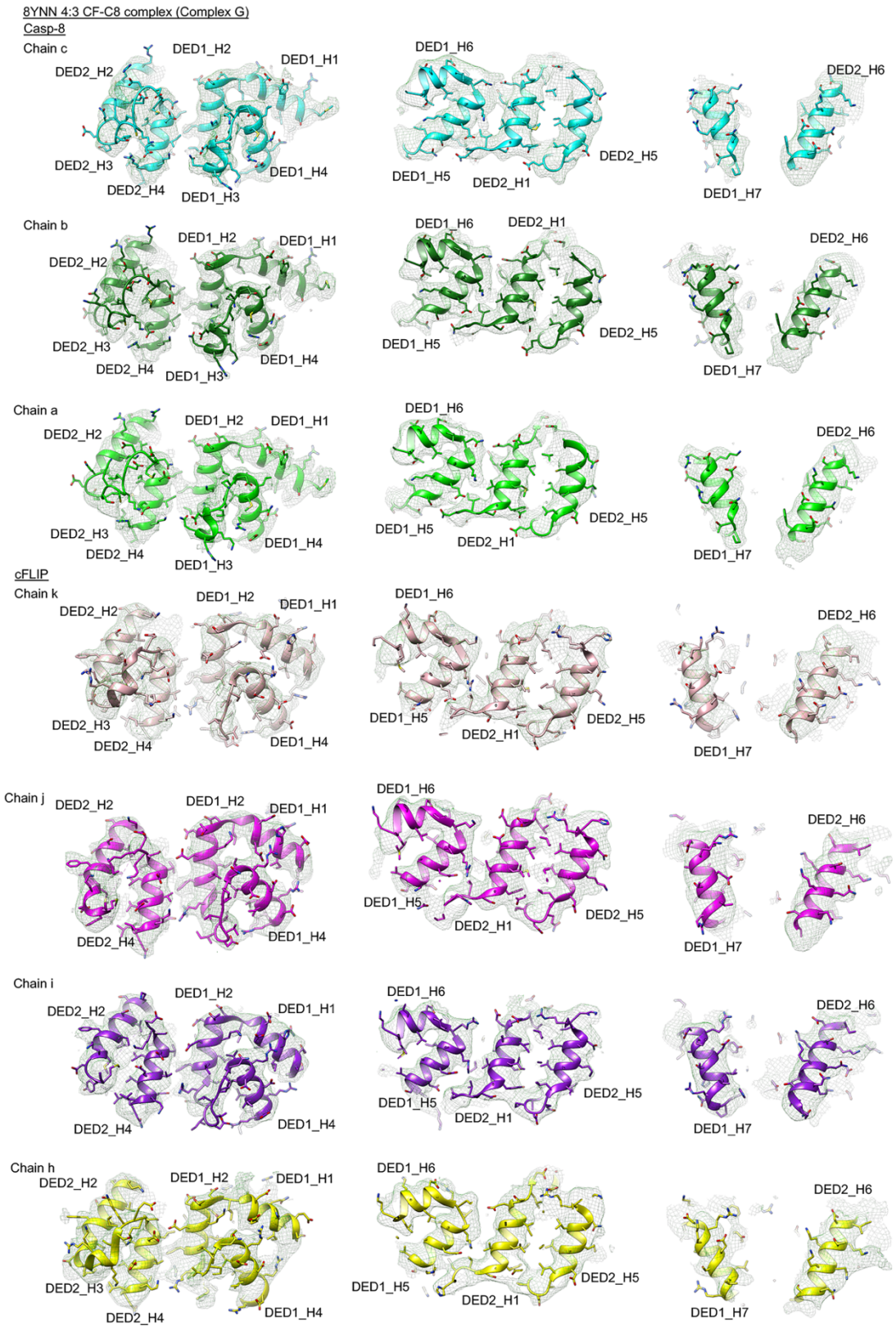

Supplementary Fig. 15: Cryo-EM maps for each helix of DED in Complex G

Shows cryo-EM maps for each helix of DED in the cryo-EM structure of 4:3 CF-C8 complex (Complex G). The contour level of the surface: 0.20-0.22 using UCSF Chimera version 1.16-42360.

Supplementary Tables

Supplementary Table 1: X-ray data collection, phasing and refinement statistics for the binary cFLIP-Casp-8 tDED complex

	CF^{H7G}-$C8^{FGLG}$*	CF-$C8^{FGLG}$*	CF^{H7G}-$C8^{FGLG}$ (Se)*
Data collection			
Space group	P21 21 21	I222	P21 21 21
Cell dimensions			
a, *b*, *c* (Å)	82.147, 166.224, 179.415	150.311, 158.640, 353.286	82.266, 167.448, 179.490
α, β, γ (°)	90.00, 90.00, 90.00	90.00, 90.00, 90.00	90.00, 90.00, 90.00
			Peak
Wavelength	1.00000	1.00000	0.97942
Resolution (Å)	50.00-2.09 (2.16-2.09)**	30.00-3.30 (3.42-3.30)	30.00-2.34 (2.42-2.34)
R_{sym} or R_{merge}	0.054 (0.279)	0.093 (0.739)	0.094 (0.358)
$I / \sigma I$	21.459 (4.252)	12.757 (1.391)	22.935 (3.354)
Completeness (%)	98.6 (95.1)	96.8 (94.8)	97.9 (88.0)
Redundancy	3.7 (3.5)	3.3 (2.8)	7.6 (6.8)
Refinement			
Resolution (Å)	32.88-2.09 (2.11-2.09)	29.64-3.30 (3.35-3.30)	29.84-2.34 (2.37-2.34)
No. reflections	143,410 (4,052)	61,336 (2,366)	102,214 (2,780)
R_{work} / R_{free}	0.1937/0.2313	0.2183/0.2643	0.2056/0.2525
No. atoms			
Protein	14,887	18,608	14,567
Ligand/ion	-	-	1
Water	466	-	51
B-factors			
Protein	46.28	137.82	50.24
Ligand/ion	-	-	112.3
Water	39.67	-	33.46
R.m.s deviations			
Bond lengths (Å)	0.008	0.002	0.005
Bond angles (°)	1.14	0.56	0.71
PDB ID	8YM5	8YM6	8YM4

*One crystal used for each data set.
**Values in parentheses are for highest-resolution shell.

Supplementary Table 2: SAXS data statistics for the CF-C8^{FGLG} complex

Sample details	
Organism	Human
source	*E. coli* expressed
UniProt sequence ID (residues in construct)	Q14790(1-185); O15519(1-181)
Extinction coefficient [A 280, 0.1%(w/v)]	0.322
Protein partial specific volume ($cm^3\ g^{-1}$)	0.7666
Particle contrast, $\Delta\rho$ [$\rho_{protein} - \rho_{solvent}$; $10^{10}\ cm^{-2}$]	2.3867 [11.8595 - 9.4728]
M_r (Da) from chemical composition	278,418
C (mol/cm^3)	0.1947
Buffer solution	20 mM Tris-HC1 pH 8.0, 80 mM NaCl
SAS data collection parameters	
Instrument	Synchrotron 23A SWAXS endstation of NSRRC
Beam geometry	0.5 mm diameter beam
Wavelength (Å)	0.82825
q-range ($Å^{-1}$)	0.0112-0.3758
Exposure time	300s with 30s single exposure time for 10 successive exposures
Concentration range (mg mL^{-1})	9.0
Temperature (K)	288
Data processing	
Primary data reduction	NSRRC 23A SWAXS package
Data processing	*ATSAS* 2.8.1; *RAW* 2.2.2
Ab initio analysis	*RAW* 2.2.2, *ATSAS 3.2.1 (r14885)*
Extinction coefficient estimate	*ProtParam*
Validation and averaging	n/a
Rigid-body modelling	n/a
Computation of model intensities	*RAW* 2.2.2
Model χ^2	*1.79*
Three-dimensional graphics representation	*PyMOL*
Structural parameters	
Guinier analysis	
$I(0)$ (cm^{-1})	1.4285 ± 0.00209
R_g (Å)	45.6500 ± 0.1086
q_{min} ($Å^{-1}$)	0.01118
qR_g max (q_{min} = 0.01118 $Å^{-1}$)	1.2901
Coefficient of correlation, R^2	0.9983
M_r (Da) from *I(0)* (*ratio to calculated M*)	286,000 (1.03)
$P(r)$ analysis	
$I(0)$ (cm^{-1})	1.4108 ± 0.000298
R_g (Å)	44.9107 ± 0.0199
D_{max} (Å)	171.6183 ± 0.4020
q range ($Å^{-1}$)	0.0112-0.3758
χ^2 fit *(estimate from RAW)*	2.2830
M_r (Da) from *I(0) (ratio to calculated M)*	282,000 (1.01)
M_r (Da) from V_P (V_P*/calculated M)*	265,200 (0.95)

Supplementary Table 3: Cryo-EM data collection, refinement and validation statistics for studying the CF-C8^{FuL_FGLG_CADA}-FA^{FuL_F25G} complex

	Complex C (EMD-39424) (PDB 8YNI)	Complex D (EMD-39425) (PDB 8YNK)	Complex E (EMD-39426) (PDB 8YNL)	Complex F (EMD-39427) (PDB 8YNM)	Complex G (EMD-39428) (PDB 8YNN)
Data collection and processing					
Magnification	165K	165K	165K	165K	165K
Voltage (kV)	300	300	300	300	300
Electron exposure (e^{-}/Å^2)	~73	~73	~73	~73	~73
Defocus range (μm)	-0.5 ~ -2.5	-0.5 ~ -2.5	-0.5 ~ -2.5	-0.5 ~ -2.5	-0.5 ~ -2.5
Pixel size (Å)	0.84	0.84	0.84	0.84	0.84
Symmetry imposed	C1	C1	C1	C1	C1
Initial particle images (no.)	246,000	246,000	246,000	246,000	246,000
Final particle images (no.)	24,014	22,967	27,558	28,464	17,838
Map resolution (Å)	3.66	3.62	3.55	3.49	3.97
FSC threshold	0.143	0.143	0.143	0.143	0.143
Map resolution range (Å)	2.5~6.1	2.3~6.6	2.3~10.9	2.0~6.2	2.6~6.8
Refinement					
Initial model used (PDB code)					
Model resolution (Å)	3.66	3.62	3.55	3.49	3.97
FSC threshold	0.143	0.143	0.143	0.143	0.143
Map sharpening *B* factor (Å^2)					
Model composition					
Non-hydrogen atoms	13,550	11,564	12,977	15,663	10,129
Protein residues	1,657	1,409	1,583	1,913	1,233
Ligands	-	-	-	-	-
B factors (Å^2)					
Protein	151.23	132.02	120.69	152.56	201.56
Ligand	-	-	-	-	-
R.m.s. deviations					
Bond lengths (Å)	0.002	0.002	0.002	0.002	0.001
Bond angles (°)	0.400	0.399	0.382	0.393	0.364
Validation					
MolProbity score	1.31	1.43	1.28	1.42	1.23
Clashscore	5.64	4.91	5.24	5.17	4.50
Poor rotamers (%)	0	0	0	0	0
Ramachandran plot					
Favored (%)	97.97	96.97	98.08	97.24	98.35
Allowed (%)	2.03	3.03	1.92	2.76	1.65
Disallowed (%)	0	0	0	0	0

Supplementary References

1 Yang, C. Y. *et al.* Deciphering DED assembly mechanisms in FADD-procaspase-8-cFLIP complexes regulating apoptosis. *Nat Commun* **15**, 3791, doi:10.1038/s41467-024-47990-2 (2024).

2 Schneider, C. A., Rasband, W. S. & Eliceiri, K. W. NIH Image to ImageJ: 25 years of image analysis. *Nat Methods* **9**, 671-675, doi:10.1038/nmeth.2089 (2012).

3 Carrington, P. E. *et al.* The structure of FADD and its mode of interaction with procaspase-8. *Mol Cell* **22**, 599-610, doi:10.1016/j.molcel.2006.04.018 (2006).